RESEARCH ARTICLE

Batteries

Energy & Environmental Materials WILEY

Deciphering the Role of $LiClO_4$ Salt on Electrochemical Properties of Plasticized Biopolymer Electrolytes for Superior EDLC Efficiency at Elevated Temperatures

*Riyadh Abdekadir Khellouf**, *Vipin Cyriac*, *Constantin Bubulinca*, *and Vladimir Sedlarik*

The advancement of electric double-layer capacitors capable of operating beyond standard conditions is vital for meeting the demands of modern electronic applications. To realize this, huge efforts have been devoted to the development of biopolymer-based electrolytes. This study explores the potential application of a plasticized biopolymer-based electrolyte in electric double-layer capacitor systems at ambient and elevated temperatures. A plasticized Na CMC/PEO/$LiClO_4$ electrolyte is successfully synthesized via a solution-casting approach. Fourier-transform infrared spectroscopy and X-ray diffraction verify the material's chemical and amorphous structure, respectively. The sample was designated as R20, with a salt concentration of 20 wt. % exhibits good electrochemical properties, including a high ionic conductivity of 3.73×10^{-4} S cm^{-1} and a wide electrochemical stability window of 3.2 V. The sample is placed into an electric double-layer capacitor cell and subjected to cyclic voltammetry and galvanostatic charge–discharge analyses at both room and high temperatures. The cyclic voltammetry test demonstrates that the electric double-layer capacitor achieves a specific capacitance (C_p) of 38 F g^{-1} at ambient temperature, which increases to 60 F g^{-1} at 60 °C. Additionally, the electric double-layer capacitor cell maintains consistent performance, demonstrating stable power and energy densities of 25 W kg^{-1} and 6 Wh kg^{-1}, respectively, under both ambient and elevated temperatures.

1. Introduction

Energy storage devices (ESDs), such as batteries and supercapacitors, have been extensively developed to meet the increasing energy demands of modern society.[1] Advancements in cathode, anode, and electrolyte materials are essential for the sustainable progression of these technologies.[2] Among these components, electrolytes play an important role in determining the overall performance of storage systems. Currently, most ESDs utilize liquid electrolytes, which suffer from inherent limitations, such as a low electrochemical stability window (ESW), restricted operating temperature range, and significant safety concerns related to flammability and volatility.[3] These challenges underscore the urgent need for alternative electrolyte materials to enhance the efficiency and safety of next-generation ESDs.[4]

Biopolymers such as starch, pectin, gum, cellulose, agar, and carrageenan have emerged as promising candidates to be used as electrolytes due to their biodegradability, non-toxicity, sustainability, and ability to operate over broader temperature and voltage ranges.[5–9] The development of bio-based solid electrolytes aligns directly with the United Nations Sustainable Development Goal (SDG) 7, which advocates for universal access to affordable, reliable, sustainable, and clean energy.[10] Additionally, this development supports the objectives of the European Green Deal's Zero Pollution Action Plan by encouraging the adoption of eco-friendly and non-hazardous materials as safer alternatives to the toxic substances typically found in liquid electrolytes.[11] Accomplishing these goals requires the creation of an innovative system in which biomaterials, such as sodium carboxymethylcellulose (Na CMC), can play a key role. Na CMC possesses a high density of carboxyl (–COO) and hydroxyl (–OH) groups along its polymeric backbone, allowing for hydrogen bonding and serving as potential complexation sites for salt ions.[12] Developing high-performance Na CMC-based electrolytes is perceived to be challenging, particularly the ionic conductivity, which needs to exceed 10^{-4} S cm^{-1}.[13] Polyethylene oxide (PEO) is widely utilized as a polymer electrolyte in ESDs owing to its good ionic conductivity, facilitated by numerous oxygen atoms. These atoms can dissolve salts by forming weak interactions that support ion transport.[14] However, PEO exhibits poor biodegradability, which poses significant environmental concerns regarding its disposal after use.[15] To address this limitation, researchers have developed a new promising approach known as polymer blending, which connects the limitations of PEO with the advantages of Na CMC. This blending has the potential to significantly boost ionic conductivity while reducing the environmental impact.[16] It is worth noting that ionic conductivity can be further enhanced

R. A. Khellouf, C. Bubulinca, V. Sedlarik
Centre of Polymer Systems, University Institute, Tomas Bata University in Zlin, Tr. T. Bati 5678, Zlin 760 01, Czech Republic
E-mail: khellouf@utb.cz
V. Cyriac
Department of Physics, Manipal Institute of Technology, Manipal Academy of Higher Education, Manipal 576104, Karnataka, India
The ORCID identification number(s) for the author(s) of this article can be found under https://doi.org/10.1002/eem2.70023.

DOI: 10.1002/eem2.70023

through the incorporation of plasticizers such as glycerol, which possess high dielectric constants and low molecular weights. These properties allow plasticizers to create alternative ion pathways, thereby increasing ionic mobility.[17] Recently, plasticized biopolymer electrolytes-based electric double-layer capacitors (EDLCs) have gained significant attention,[18–23] due to their excellent power density, rapid charge–discharge capabilities, and long cycling lifespan. The carboxymethyl cellulose (CMC) membrane electrolyte has been successfully tested for large-scale production using an upscaled process that involves dissolving, casting, drying, and soaking. However, its compatibility with industrial EDLC manufacturing standards may present certain challenges, particularly in achieving optimal electrode-electrolyte interfacial integration in commercial EDLC cells; addressing these limitations requires further optimization of the electrolyte and processing techniques to enhance adhesion and ionic transport at the interface.[24] Moreover, the plasticized biopolymer electrolytes-based EDLCs performance under elevated temperature remains underexplored. This gap in the literature serves as motivation for developing temperature-tolerant supercapacitor-based plasticized electrolytes. In line with this objective, this study aims to create a novel plasticized electrolyte system consisting of Na CMC, PEO, and glycerol, with various concentrations of $LiClO_4$ as the dopant. The resulting Na CMC/PEO/$LiClO_4$ system was subjected to a comprehensive series of analyses including Fourier-transform infrared (FTIR) spectroscopy, electrochemical impedance spectroscopy (EIS), X-ray diffraction (XRD), scanning electron microscopy (SEM), and linear sweep voltammetry (LSV). Additionally, dielectric analyses were employed to probe the underlying relaxation processes, and thermogravimetric analysis (TGA) was utilized to determine thermal stability. The sample with the highest ionic conductivity was chosen for incorporation into an EDLC cell. Its electrochemical characteristics were evaluated using cyclic voltammetry (CV) and galvanostatic charge–discharge (GCD) measurements under both ambient and elevated temperatures, offering valuable insights into its suitability for energy storage applications.

1.1. Characterizations of the Prepared Polymer Blend Electrolytes (PBEs)

Fourier-transform infrared spectroscopy measurements were conducted using an iS5 spectrometer, spanning a wavenumber range of 600–4000 cm^{-1}. XRD analysis was performed with a Rigaku MiniFlex 600 desktop diffractometer employing Cu Kα radiation, scanning from 3° to 90° (2θ) at a rate of 5° min^{-1}. Surface topography was examined via a Phenom Pro desktop scanning electron microscope (SEM) at a magnification of 1000×. In addition, thermogravimetric analysis (TGA) was carried out on a TA Q500 analyzer over a temperature range of 25–800 °C under nitrogen flow (20 mL min^{-1}).

1.2. Electrochemical Measurements and Analysis of PBEs

A PG STAT 128 N Potentiostat/Galvanostat was employed to determine the ionic conductivity and electrical characteristics of the plasticized Na CMC/PEO/$LiClO_4$ electrolytes. Disc-shaped plasticized PBE samples, each with a 1.6 cm diameter, were positioned within a Swagelok cell. An AC signal of 10 mV amplitude was then applied, while sweeping frequencies from 10 Hz to 500 kHz, to assess the impedance behavior of the system. Bulk conductivity (σ) was calculated using the following Equation (1):

$$\sigma = \frac{t}{R_b A} \tag{1}$$

Here R_b is the bulk resistance, A is the contact area between the polymer electrolyte film and the electrodes, which is estimated to be 2.096 cm^2, and t refers to the thickness of the electrolyte film, as mentioned in Table 3. The previously described setup was utilized to perform the linear sweep voltammetry (LSV) test. Sample designated as R20 was placed in a Swagelok cell and tested over a voltage range of 0–5 V with a scan rate of 5 mV s^{-1}. To gain insight into the electrolyte ion dynamics behavior and tangent loss, EIS data were transformed into a dielectric format using Equations (2–4).

$$\epsilon' = \frac{Z_i}{\omega C_0 \left(Z_r^2 + Z_i^2\right)} \tag{2}$$

$$\epsilon'' = \frac{Z_r}{\omega C_0 \left(Z_r^2 + Z_i^2\right)} \tag{3}$$

$$\tan\delta = \frac{\epsilon''}{\epsilon'} \tag{4}$$

ϵ' and ϵ'' represent the real and imaginary parts of complex permittivity, respectively. ω is the angular frequency, calculated as 2πf and C_0 is vacuum capacitance.

The ion transport parameters (D, μ, and n) are obtained by the Arof-Noor method[25] by fitting the Nyquist plot using the electrical equivalent circuit (EEC) and transport parameters obtained by using Equation (5):

$$D = \frac{\left(k_2 \epsilon' \epsilon_0 A\right)^2}{\tau_2} \tag{5}$$

where D is the diffusion coefficient, k_2^{-1} is the capacitance of the electric double layer formed at the electrode-electrolyte interface, ϵ' is the dielectric constant obtained from Equation (2), ϵ_0 is the vacuum permittivity, A is the electrode-electrolyte contact area, and τ_2 is a time constant corresponding to a minimum in $-Z_i$.

$$\mu = \frac{eD}{kT} \tag{6}$$

where μ is the mobility of the charge carriers, k is the Boltzmann constant (1.38×10^{-23} J K^{-1}), T is the absolute temperature in Kelvin, and e is the electron charge (1.602×10^{-19} C).

The number density of charge carriers (n) can be obtained using Equation (7):

$$n = \frac{\sigma}{e\mu} \tag{7}$$

1.3. Electrochemical Characterization of EDLC Cell

The electrochemical performance of the fabricated EDLC cell, encompassing CV and GCD analyses, was evaluated using a Bio-Logic BCS-

810 battery cycler at ambient and higher temperatures. CV tests were carried out within a voltage range of 0–1 V at various scan rates of 5, 10, 20, 40, 80, and 100 mV s^{-1}, while GCD measurements were performed at a current density of 0.05 A g^{-1}.

EIS was performed to analyze the electrical properties at the interfaces of the EDLC cell. This measurement was performed at an AC voltage of 10 mV over a frequency range of 10 Hz–100 kHz. The specific capacitance was calculated using Equations (8) and (9).

$$C_p = \frac{2 \times \int IdV}{m\, v \Delta V} \tag{8}$$

$$C_p = \frac{i}{m} \times \frac{\Delta t}{\Delta V} \tag{9}$$

C_p represents the specific capacitance, which was calculated from the CV curve. The term $\int IdV$ denotes the area under the CV curve, where m is the combined mass of both electrodes (0.02 g), v is the scan rate, and ΔV is the potential window. Additionally, i representing the applied current (0.8 mA), m refers to the mass of active material in both electrodes, Δt indicating the discharge time, and ΔV denoting the potential change during discharge.

The energy density E_d, power density P_d, equivalent series resistance ESR, and coulombic efficiency (η) of the EDLC cell were calculated using the following Equations (10–13):[7,26]

$$E_d = \frac{0.5 \times C_p\, (\Delta V)^2}{3.6} \tag{10}$$

$$P_d = \frac{E \times 3600}{\Delta t} \tag{11}$$

$$ESR = \frac{V_{drop}}{i} \tag{12}$$

$$\eta = \frac{t_d}{t_c} \times 100\% \tag{13}$$

V_{drop} represents the voltage drop, t_d denotes the discharging time, and t_c corresponds to the charging time.

2. Results and Discussion

2.1. Structural Analysis of PBEs

Figure 1a shows the FTIR spectra of pristine PEO and Na CMC. In the PEO spectrum, characteristic triplet peaks appear at 1058, 1092, and 1144 cm^{-1}, corresponding to C–O–C stretching vibrations. Additionally, several bands associated with CH_2 vibrational modes are present. The symmetric and asymmetric rocking modes of CH_2 appear at 840, 946, and 959 cm^{-1}, while the symmetric and asymmetric twisting modes are observed at 1240 and 1278 cm^{-1}. The CH_2 wagging mode is represented by a doublet at 1340 and 1360 cm^{-1}, whereas the asymmetric CH_2 scissoring mode is located at 1465 cm^{-1}. Finally, the symmetrical stretching vibration of CH_2 is observed at 2879 cm^{-1}.[27] By contrast, the Na CMC spectrum exhibits an absorption band at 3278 cm^{-1}, corresponding to OH stretching vibrations. The CH stretching vibration appears at 2933 cm^{-1}, while the asymmetric and symmetric stretching of the carboxylate anion ($–COO^-$) are observed at 1595 and 1416 cm^{-1}, respectively. Additionally, the OH bending vibration is present at 1325 cm^{-1}, while the peak appears at 1031 cm^{-1}, corresponding to C–O–C ether linkages.[28]

Figure 1b shows the spectra of the plasticized Na CMC/PEO blend with varying concentrations of $LiClO_4$. Notably, the OH band in the Na CMC spectrum appears at 3278 cm^{-1}. However, in the R0 spectrum, this band shifts to 3299 cm^{-1}, suggesting the formation of hydrogen bonds, primarily between the OH groups of glycerol and those within the polymer blend.[29] It is important to highlight that the conduction process primarily relies on ion hopping between the polymer blend's oxygen atoms and cations. Thus, changes in the wavenumbers associated with these atoms are considered strong evidence of the successful interaction between the polymer blends and Li^+. As shown in **Table 1**, higher concentrations of $LiClO_4$ cause the OH peak to decrease in intensity and shift towards lower frequencies, affirming the

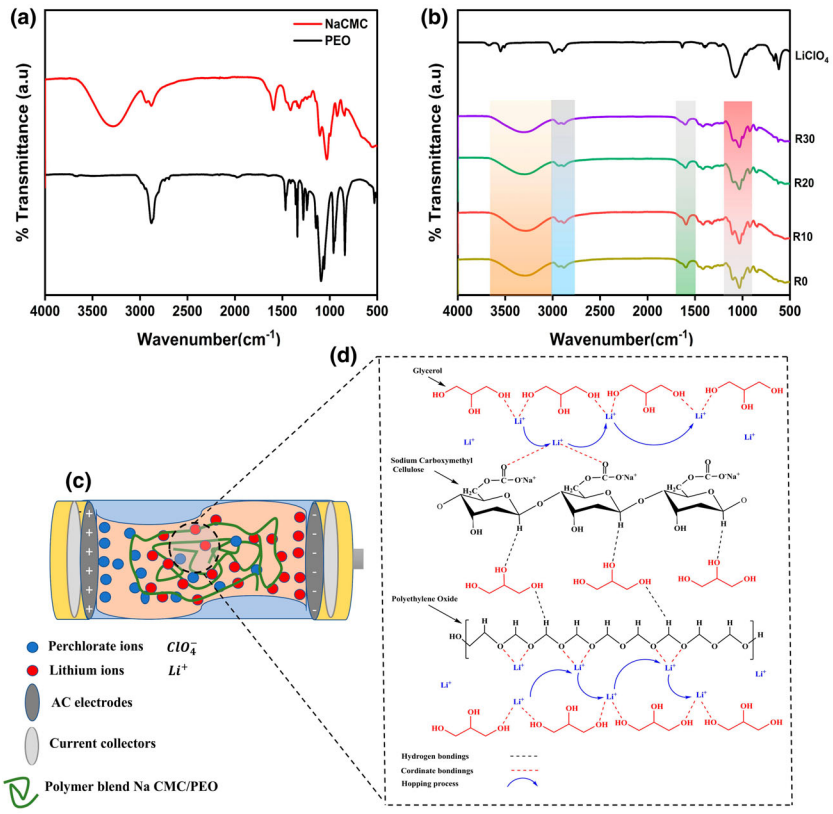

Figure 1. a) FTIR of pure PEO and Na CMC, b) plot of plasticized Na CMC/PEO doped with $LiClO_4$, c) design of the prepared EDLC, and d) proposed interactions between the PBEs.

Table 1. Key functional groups of the prepared plasticized Na CMC/PEO/$LiClO_4$ and their corresponding wavenumbers based on FTIR analysis.

Samples	Functional groups and their corresponding wavenumbers (cm^{-1})			
	C–O–C stretching	$–COO^-$ stretching	–CH stretching	–OH stretching
R0	1032	1595	2937	3299
R10	1029	1592	2933	3286
R20	1028	1592	2933	3283
R30	1032	1600	2937	3300

interaction between Li^+ and the oxygen atoms in the OH groups.[30] Additionally, the peak at 1595 cm^{-1}, attributed to the carboxylate group ($–COO^-$), moves to lower frequencies, indicating interactions between C=O groups and Li^+ cations.[31] The FTIR spectra also display a band at 1032 cm^{-1}, corresponding to the C–O–C bond, which shows a decrease in intensity and a slight shift to lower frequencies.[7] This shift can be attributed to two key interactions: first, between Li^+ cations and the oxygen atoms in the ether oxygen bond, as reported by Y. Li et al.,[32] and second, between Li^+ cations and the oxygen atoms in the glycosidic linkages of Na CMC, as noted by Hamsan et al.[33] Collectively, the changes in band intensities and shifts in their positions confirm the interactions between the salt and plasticized Na CMC/PEO blend, as illustrated in Figure 1d.

XRD analysis was performed to investigate the crystal structure of the plasticized Na CMC/PEO/$LiClO_4$ system. **Figure 2**a shows the XRD diffractograms of pure $LiClO_4$, PEO, and Na CMC. $LiClO_4$ displays intense, sharp peaks at $2\theta = 24°$, 27°, 28°, 30°, 36°, and 38°, indicating its crystalline structure.[34] Similarly, PEO exhibits characteristic crystalline peaks between 17° and 31°.[35,36] By contrast, Na CMC exhibited an amorphous structure with no sharp diffraction peaks.

Figure 2b shows the X-ray diffractogram of the plasticized Na CMC/PEO blend with varying $LiClO_4$ concentrations. Notably, sample R0 shows an absence of crystalline peaks associated with PEO, due to interactions between glycerol, PEO, and Na CMC.[37] These interactions disrupted the regular PEO chain arrangement and created a broad hump at $2\theta = 24°$, demonstrating the presence of a predominantly amorphous phase within the material. Samples R10, R20, and R30 exhibited similar patterns with varying peak intensities and widths. Increasing the $LiClO_4$ concentration further reduced the intensity and broadened the peak, indicating an expanding amorphous phase. This trend suggests that higher salt concentrations disrupt intermolecular interactions within the Na CMC/PEO matrix, leading to structural rearrangements and reduced crystallinity.[38] Crystallinity levels were quantified using the deconvolution method with the Fityk[39] (see **Figure 3**).

Figure 3 represents the deconvoluted XRD spectrum of the plasticized Na CMC/PEO/$LiClO_4$ blend, showing four broad amorphous peaks[40] and a crystalline peak at $2\theta = 24°$, which corresponds to the (200) crystallographic plane.[2] After incorporating various concentrations of $LiClO_4$, the intensity of the amorphous peaks increases, while the crystalline peak intensity decreases.[40] The degree of crystallinity (χ) is calculated using Equation (14):

$$\chi = \frac{A_c}{A_c + A_a} \times 100\% \quad (14)$$

Here, A_c refers to the areas under the crystalline peaks while A_a represents the areas under the amorphous peaks.

Figure 3 shows that the initial crystallinity of sample R0 was 9.95%, which decreased to 6.94% and 5.61% for samples R10 and R20, respectively. Interestingly, sample R30 exhibits a slight increase in crystallinity, likely due to the reassociation of the dissociated Li^+ and ClO_4^- ions to form ion pairs, contributing to this observed trend.[41]

2.2. Electrochemical Properties of PBEs

EIS was conducted to assess the ionic conductivity of the plasticized Na CMC/PEO/$LiClO_4$ system, focusing on both bulk material properties and interfacial behavior.[42] **Figure 4**a shows Nyquist plots of the plasticized Na CMC/PEO/$LiClO_4$. The Nyquist plots exhibit a depressed semicircle in the high-frequency region, attributed to ion mobility resistance, followed by an inclined line in the low-frequency region, which corresponds to the capacitance of the electrical double layer (EDL) formed at the electrode/electrolyte interface.[43] Figure 4a illustrates that increasing the salt concentration led to a decrease in the length of the inclined line in the Nyquist plots. This decrement can be attributed to the reduction in the effective thickness of EDL, resulting from an accumulation of ions near the electrode surface.[44] It can be seen from **Table 2** that the bulk resistance (R_b) followed a similar trend where R_b values for samples R0, R10, and R20 decrease progressively from 162.39 to 32.30 Ω, indicating an initial enhancement in the ionic conductivity. However, for sample R30, R_b slightly increases to 46.59 Ω, suggesting ion pair reassociation, which limits the number of free ions and ultimately decreases the ionic conductivity.[41] The Bulk conductivity was determined using Equation (1), and the corresponding values are listed in Table 2.

Table 2 shows that incorporating $LiClO_4$ led to a progressive improvement in the ionic conductivity of the plasticized PBEs. Sample R20 demonstrated the optimal conductivity among the doped samples.

The ion transport properties (n, μ, D) have been investigated using the Arof-Noor approach which involves fitting the Nyquist plot (**Figure 5**) using an Electrical Equivalent Circuit (EEC). The EEC used to fit the graph is shown in the inset of Figure 5.

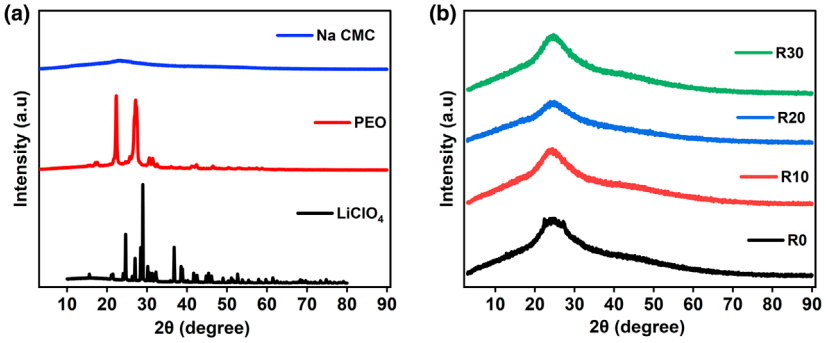

Figure 2. a) XRD diffractogram of pure $LiClO_4$, PEO, and Na CMC. b) XRD diffractogram of plasticized Na CMC/PEO/$LiClO_4$.

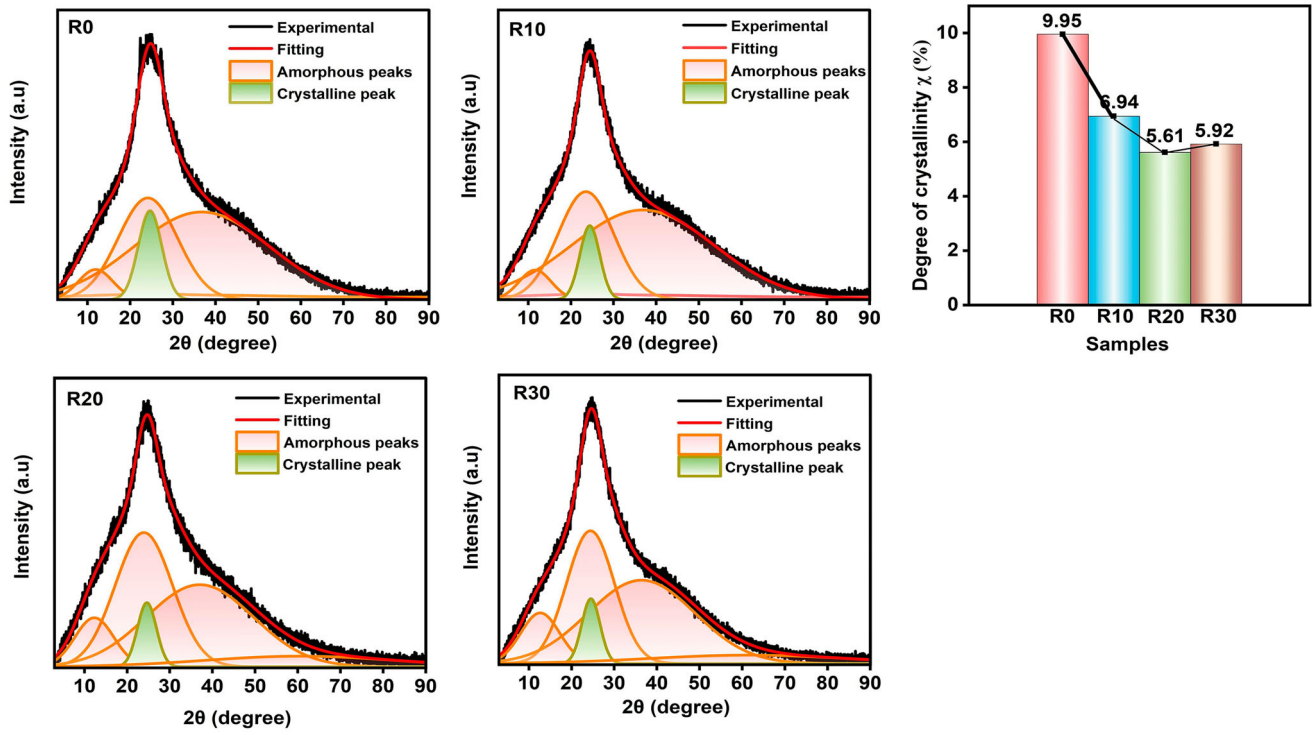

Figure 3. Deconvoluted XRD diffractogram of plasticized Na CMC/PEO/$LiClO_4$.

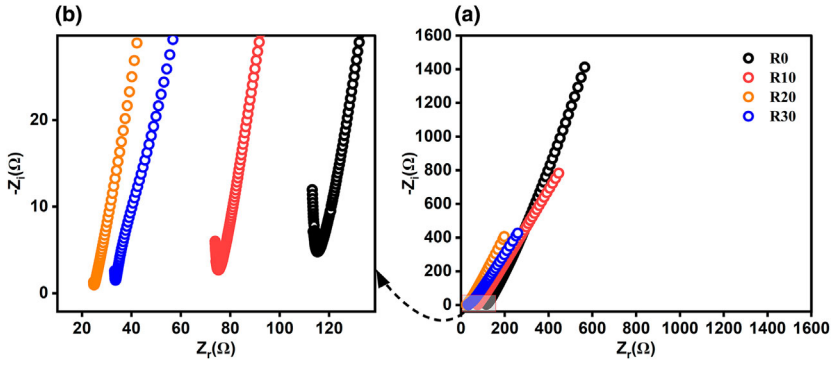

Figure 4. a) Nyquist plot for Na CMC/PEO/$LiClO_4$ polymer electrolytes, b) zoomed-in view of the high-frequency region.

The fitted parameters were used to evaluate the transport parameters listed in Table 2. It is very clear that the number density of charge carriers (n) varies just like the conductivity (σ) does. Hence n significantly influences the conductivity rather than μ and D.

Figure 6a,b show real ε′ and imaginary ε″ part of complex permittivity ε* as a function of frequency.[45] It is evident that both ε′ and ε″ exhibit increased values at lower frequency regions demonstrating the presence of electrode polarization and high density of charge carriers.[42] However, in high-frequency region, both ε′ and ε″ decrease nonlinearly. This decrease may result from either a reduction in the number of dipoles actively contributing to the electrode polarization effect or the increasing difficulty for ions to align with the applied electric field direction.[41] Figure 6c presents the loss tangent spectra (tanδ) for the Na CMC/PEO/$LiClO_4$ system. The spectra revealed a single relaxation peak, indicating a conductivity relaxation. The conductivity relaxation time (τ) was calculated using Equation (15), with values listed in Table 2.

$$2\pi f_{max}\tau = 1 \quad (15)$$

Table 2 demonstrates an inverse relationship between salt concentration and conductivity relaxation time (τ). As the salt concentration increases, the τ decreases. This reduction in relaxation time suggests an acceleration in segmental relaxation dynamics.[46]

A broad ESW is crucial for Na CMC/PEO/$LiClO_4$'s viability in EDLC cells. ESW is typically assessed using LSV. Figure 6d shows the LSV plot for the R20 sample, where a stable, negligible current was observed within the 0–3 V range. Beyond this range, the current increases nonlinearly while the potential remains stable, indicating the onset of R20 sample decomposition.[47] Generally, an ESW is identified by the point at which the extrapolated nonlinear curve intersects the potential axis. The ESW for R20 was determined to be 3.2 V, suggesting its suitability as an ideal electrolyte for EDLC.

2.3. Morphological Study

Figure 7 presents the SEM micrographs of all samples evaluated in this study. Pure PEO is known to exhibit a notably rough surface

Table 2. Bulk resistance (R_b), ionic conductivity σ, angular frequency ω_{max}, relaxation time τ, carrier density (n), mobility (μ), and diffusion coefficient (D) for prepared PBEs.

Samples	R_b (Ω)	σ (S cm^{-1})	ω_{max} (Hz)	τ (s)	n (cm^{-3})	μ (cm^2 V^{-1} s)	D (cm^2 s^{-1})
R0	162.39	8.30×10^{-5}	443 003	2.26×10^{-6}	2.81×10^{20}	1.84×10^{-6}	4.77×10^{-8}
R10	89.45	1.61×10^{-4}	585 716	1.71×10^{-6}	1.581×10^{21}	6.37×10^{-6}	1.65×10^{-8}
R20	32.30	3.73×10^{-4}	1 226 458	8.15×10^{-7}	1.93×10^{21}	1.20×10^{-6}	3.11×10^{-8}
R30	46.59	2.58×10^{-4}	884 192	1.13×10^{-6}	1.72×10^{21}	9.35×10^{-7}	2.42×10^{-8}

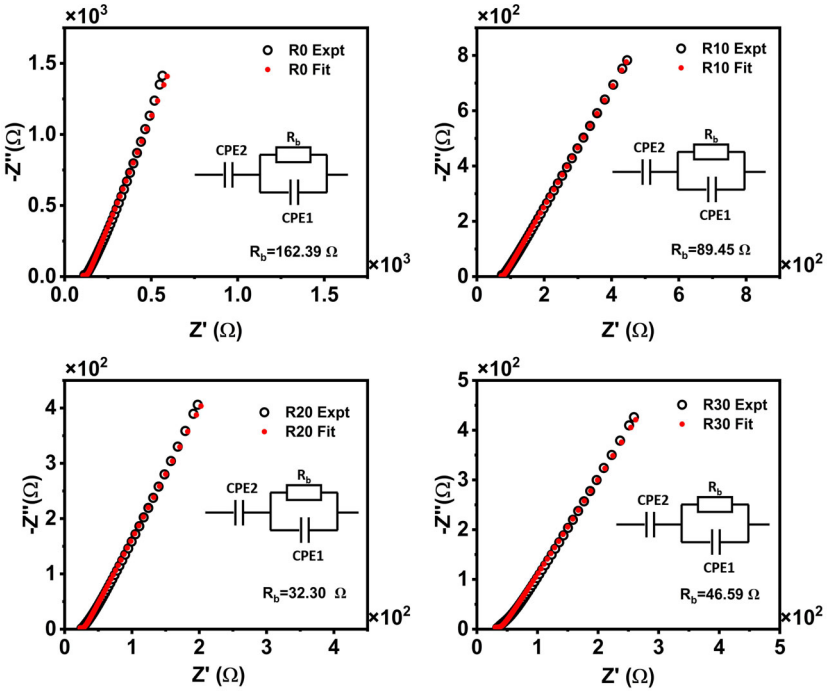

Figure 5. Nyquist plot fitted using EEC. Black circles indicate experimental data, and red dots indicate fitted data. EEC is shown as an inset.

morphology with numerous folds and wrinkles, indicating a crystalline phase within the polymer.[48] However, upon blending PEO with Na CMC, the surface became significantly smoother, as shown in Figure 7. This reduction in surface irregularities suggests an enhanced compatibility between Na CMC and PEO. A smoother electrolyte surface is generally associated with more facile ion transport, thereby contributing to elevated DC conductivity. As the salt content increases, the improved dispersion within the polymer matrix yields progressively smoother surfaces.[49] This evolution towards greater surface uniformity is directly coupled with an incremental rise in ionic conductivity, aligning well with findings from previous polymer electrolyte research.[50] Nevertheless, it is important to note that achieving such a smooth surface morphology at very high salt concentrations is not expected. In related work, Arof et al. fabricated CS: PVA: xNH_4NO_3 solid polymer electrolytes and observed a notable decrease in DC conductivity at elevated salt concentrations.[51] They attributed this behavior to the formation of ion aggregates, which protruded from the surface. A similar pattern is observed in the case of the R30 sample, due to which the ionic conductivity of this sample has dropped when compared to the R20 sample.[41]

2.4. Thermal Stability

As shown in **Figure 8**, the TGA profiles of the plasticized Na CMC/PEO/$LiClO_4$ system revealed that the R0 sample underwent three stages of thermal decomposition. The initial weight loss of approximately 21% corresponds to the evaporation of moisture absorbed by the plasticized Na CMC/PEO matrix.[52] This is followed by a significant 39% weight loss, primarily due to the release of COO^- from the decomposition of polymer side chains.[53] The final stage, accounting for roughly 14% of weight loss, aligns with the breakdown of the remaining polymer backbone and other stable components.[54] By contrast, the incorporation of $LiClO_4$, as observed in samples R10, R20, and R30, resulted in TGA curves displaying water elimination followed by a significant degradation step with a weight loss ranging from 63% to 64% and a maximum degradation temperature exceeding 174 °C. This higher thermal stability suggests the suitability of this material for EDLC applications.

2.5. Electrochemical Performance of the EDLC at Room and Elevated Temperature

CV tests for EDLC-based plasticized biopolymer electrolytes have been extensively studied at ambient temperature. However, due to the limited research at elevated temperatures, this study aims to investigate the CV performance of EDLCs at 60 °C. This approach provides valuable insights into the behavior of the prepared material under conditions that simulate real-life applications, particularly considering the unprecedented rise in global temperatures. As shown in **Figure 9**a,b, the CV plot of the EDLC cell exhibited a quasi-rectangular shape without redox peaks at both room and higher temperatures, indicating stable capacitive behavior.[55] Furthermore, the CV plot consistently retained its shape across different scan rates, supporting the reliability of Na CMC/PEO/$LiClO_4$ under different operational conditions.

The capacitance performance of the prepared EDLC cell at room and higher temperatures was determined using Equation (8). It can be seen from Figure 9c that at room temperature and lower scan rates of 5–10 mV s^{-1}, the C_p of the EDLC was observed to range between 38 and 35 F g^{-1}. Conversely, at higher temperatures under the same scan rates, the C_p increased to 60–38 F g^{-1}. This enhancement in capacitance at higher temperatures can be attributed to the improved ionic conductivity of the electrolyte. Elevated temperatures promote better ion mobility

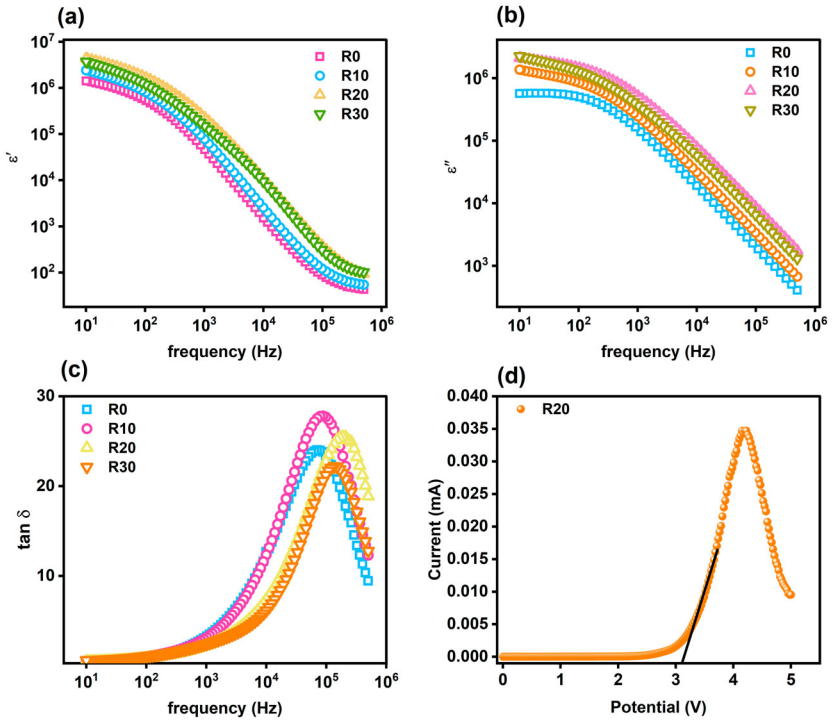

Figure 6. Variation of a) ε′, b) ε″, c) tan δ as a function of frequency for all samples and d) LSV plot for R20 sample.

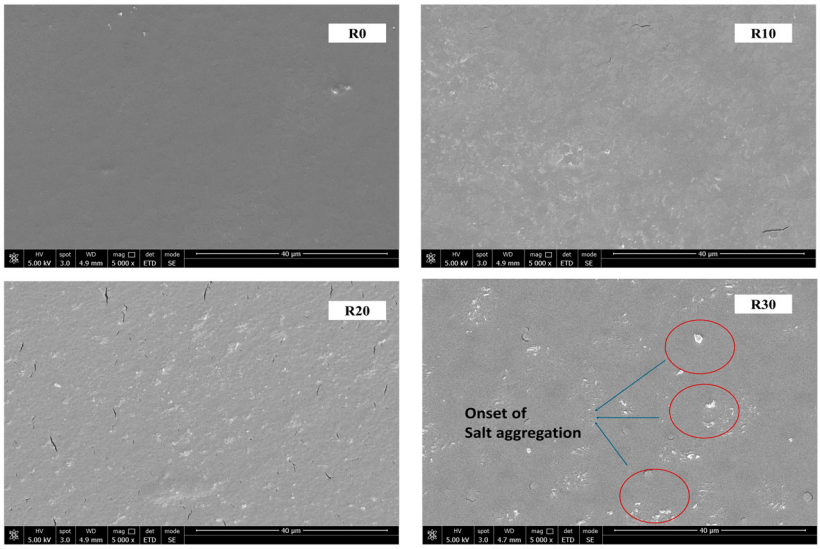

Figure 7. SEM micrographs of Na CMC/PEO/$LiClO_4$ polymer electrolytes.

within the electrolyte, enabling more efficient charge storage and resulting in higher capacitance values.[56] At higher temperatures and scan rates of 20, 40, 80, and 100 mV s^{-1}, C_p was observed to decrease progressively, with values recorded as 24, 16, 14, and 9 F g^{-1}, respectively. By contrast, at room temperature and the same scan rates, C_p showed higher values of 35, 23, 18, and 16 F g^{-1}. This reduction in capacitance at elevated temperatures can be primarily attributed to thermal agitation, a phenomenon driven by the random movement of atoms and molecules.[57] Thermal agitation disrupts the orderly motion of ions, reducing their ability to effectively adsorb onto the electrode surface and thereby decreasing the overall charge storage efficiency of the EDLC cell.

The EDLC cell was subjected to a current density of 0.05 A g^{-1}. As shown in Figure 9d, the initial C_p was recorded at 6 F g^{-1}. However, it progressively increased, reaching a peak value of 44 F g^{-1} by cycle number 700. This behavior can be correlated with ion agglomeration, which initially restricts ion mobility but gradually stabilizes as the system undergoes repeated cycling.[7] Beyond cycle 700, C_p remained stable until the end of the GCD process, demonstrating that the EDLC cell achieved and maintained consistent charge storage performance.

The coulombic efficiency followed similar trends to the C_p, maintaining a consistent 100% efficiency over 5000 cycles. Notably, the EDLC exhibited a low voltage drop, as reflected in the equivalent series resistance (ESR). As shown in Figure 9e, the initial ESR value was 75 Ω, which decreased to 17 Ω and remained stable until the end of the GCD process. This reduction in ESR indicates an improvement in ion mobility from the electrolyte to the electrode surfaces, enabling the EDLC cell to retain its full practical functionality over an extended period.[58] In short, the EDLC cell demonstrated good electrochemical performance, as evidenced by the obtained energy density of 6 Wh kg^{-1} and power density of 25 W $kg;^{-1}$ see Figure 9f.

The GCD test at higher temperatures is perceived as one of the most reliable tests for evaluating the stability and performance of EDLCs under harsh conditions. In this study, the GCD test was conducted at 60 °C for 1000 cycles. This test provides valuable insights into the capacity of the electrolyte to maintain its functionality under challenging conditions. As shown in **Figure 10a**, the GCD curve at 60 °C exhibited a triangular pattern with a longer discharge time. Figure 10b further illustrates that the initial C_p was observed at 23 F g^{-1} which is fourfold higher than the value determined at room temperature. The C_p increased progressively throughout cycling, reaching a value of 47 F g^{-1} at 700 cycles. This increment can be attributed to the enhanced diffusion of ions within the electrolyte system driven by the effect of higher temperatures.[59] By simplifying the structural complexities of the plasticized electrolyte, the Stokes-Einstein equation is given by Equation (16).

$$D = \frac{kT}{6\pi r\eta} \tag{16}$$

where k is the Boltzmann constant, T is the temperature, r is the ionic radius, η is the viscosity, and D is the diffusion coefficient,

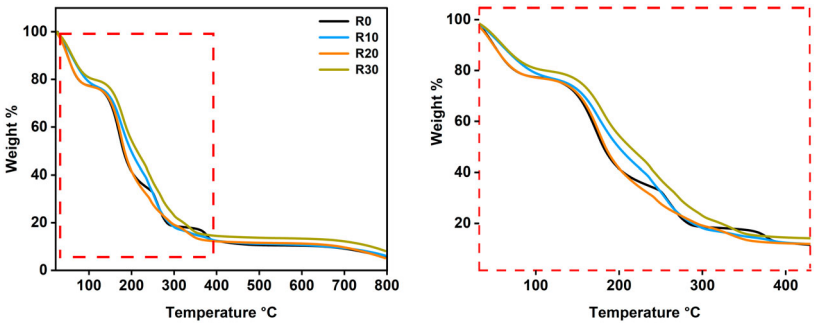

Figure 8. TGA thermograms of plasticized Na CMC/PEO/$LiClO_4$.

which describes the relationship between diffusion and temperature.[59] According to this equation, diffusion is directly proportional to temperature T. As the temperature increased, diffusion was significantly enhanced, allowing ions to access the electrode surface more efficiently. This phenomenon contributes to the observed increase in C_p. Notably, after 700 cycles, C_p decreased slightly, reaching 37 F g^{-1} after 1000 cycles. This reduction can be associated with the gradual drying of the electrolyte. Similar findings were reported by Sun et al.[60]

EIS measurements were conducted at room and elevated temperatures to validate the previously mentioned claims. As shown in Figure 8d, at room temperature, the R_b and charge transfer resistances (R_{ct}) were determined as 50 and 1.47 Ω, respectively. At 60 °C, these values decreased significantly, with R_b and R_{ct} observed at 11.8 and 0.57 Ω, respectively. This reduction in R_{ct} confirms an improvement in ion diffusion at higher temperatures.[55] Generally, the R_{ct} reflects the resistance encountered during the transfer of ions at the interface between the electrolyte and the electrode surface.[7] Evaluating the overall performance of the prepared electrolyte at elevated temperatures, Figure 10c shows that the EDLC cell at 60 °C achieved a maximum energy density of 6 Wh kg^{-1} and a power density of 25 Wkg^{-1}. These

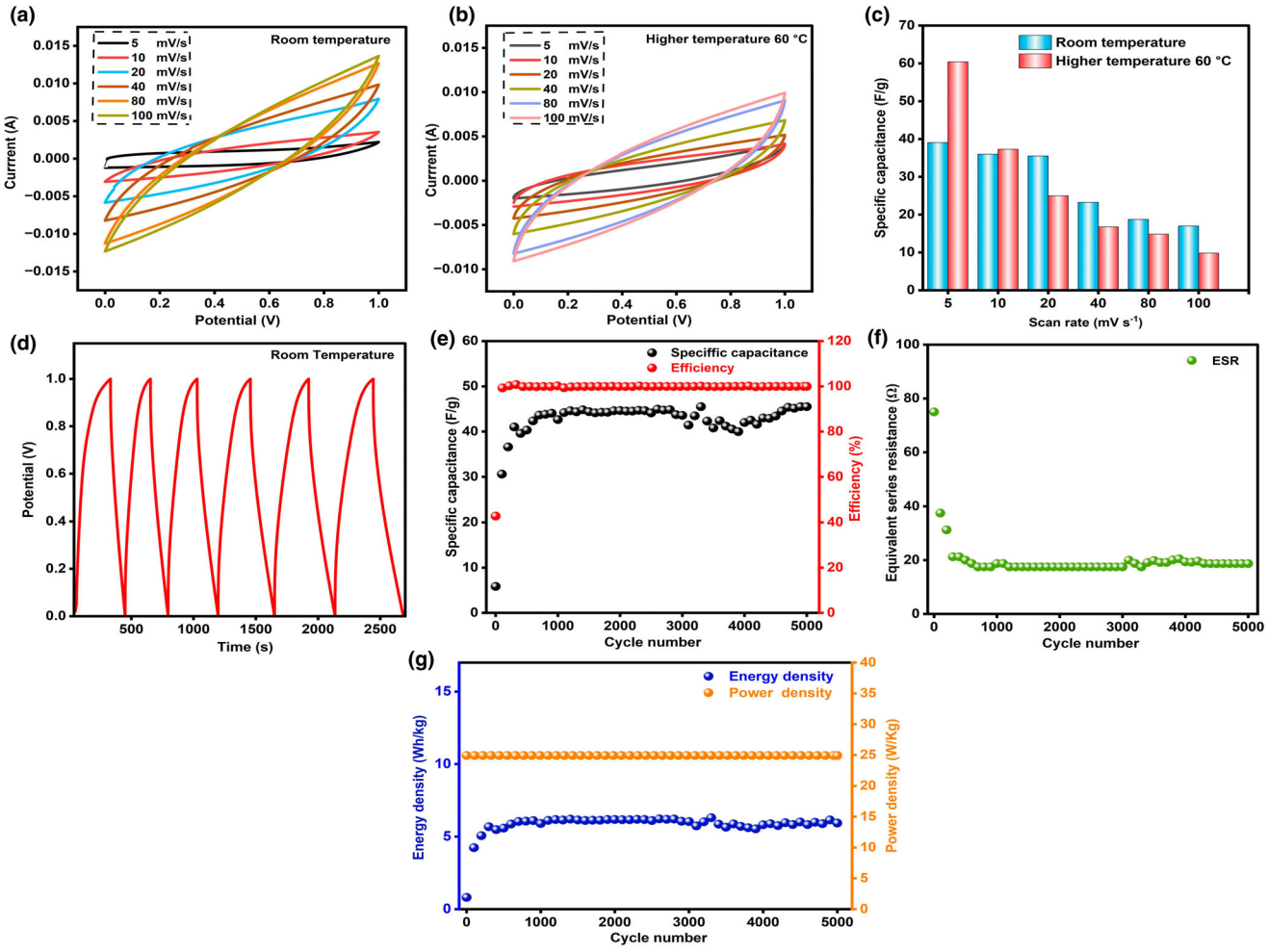

Figure 9. a) CV curves of the EDLC cell at various scan rates at room temperature. b) CV profiles of the EDLC cell at different scan rates under elevated temperature. c) C_p values derived from CV analysis at both room and elevated temperatures. d) GCD curves for the initial cycles. e) C_p and efficiency as a function of cycle number. f) ESR variation over 5000 cycles and g) energy density and power density for the EDLC cell at room temperature.

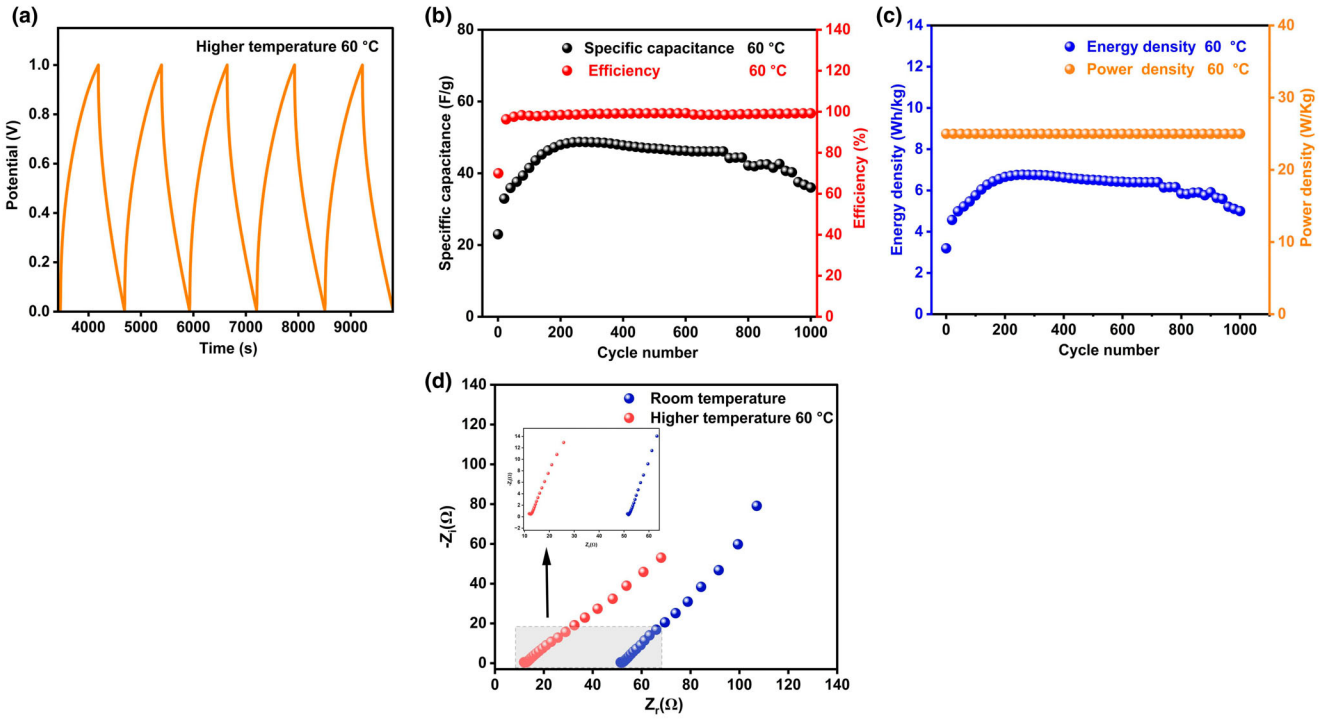

Figure 10. a) GCD curves for the initial cycles at 60 °C. b) C_p and efficiency η as a function of cycle number at 60 °C. c) Energy density and power density for the EDLC cell and d) EIS of the EDLC cell at room and higher temperatures.

Table 3. Composition details of plasticized Na CMC/PEO/$LiClO_4$ electrolyte films.

Sample	Na CMC (wt. %)	PEO (wt. %)	$LiClO_4$ (g) (wt. %)	Thickness of electrolyte films (mm)
R0	80	20	0	0.0271
R10	80	20	10	0.0290
R20	80	20	20	0.0242
R30	80	20	30	0.0242

findings highlight the good electrochemical performance of the EDLC cell at 60 °C.

3. Conclusion

A new plasticized Na CMC/PEO/$LiCLO_4$-based electrolyte has been successfully prepared, demonstrating a good ionic conductivity of 3.73×10^{-4} S cm^{-1} and a wide ESW of 3.2 V. These outstanding electrochemical properties enable the effective integration of this material into EDLC applications.

The assembled EDLC cell with NaCMC/PEO/$LiClO_4$ exhibited stable and reliable electrochemical performance at ambient temperature, as reflected in the achieved specific capacitance of 44 F g^{-1} over 5000 cycles, along with maximum energy and power densities of 6 Wh kg^{-1} and 25 W kg^{-1}, respectively. While some biopolymer-based electrolytes may exhibit higher capacitance, they often suffer from poor cycling stability or limited temperature resistance. However, a key advantage of our electrolyte system is its enhanced thermal stability. To the best of our knowledge, many high-capacitance biopolymer-based EDLCs have not been tested under elevated temperatures, raising concerns about their performance in harsh conditions. In contrast, our electrolyte exhibits good thermal stability, ensuring consistent and reliable performance at higher temperatures. At 60 °C, the EDLC cell maintained a maximum specific capacitance of 47 F g^{-1}, with energy and power densities comparable to those observed at room temperature. These results highlight the potential use of the prepared electrolyte for EDLC application at both ambient and elevated temperatures. However, further investigations are needed to evaluate the long-term performance and stability of the Na CMC/PEO/$LiClO_4$-based EDLC under extended exposure to elevated temperatures during prolonged GCD tests.

4. Experimental Section

Materials: All chemical reagents, including sodium carboxymethyl cellulose (Na CMC, $M_w \approx 250\,000$ g mol^{-1}), glycerol (99%, $M_w \approx 92$ g mol^{-1}), PEO ($M_w \approx 600\,000$ g mol^{-1}), *N*-methyl-2-pyrrolidone (99% NMP, $M_w \approx 99.13$ g mol^{-1}), and high-purity lithium perchlorate (99.9% $LiClO_4$, $M_w \approx 106.39$ g mol^{-1}), were sourced from Sigma-Aldrich, Germany. Additionally, activated carbon with a specific surface area of approximately 1670 m^2 g^{-1}, carbon black and a polytetrafluoroethylene (PTFE) binder were obtained from MSE Supplies LLC, USA.

Preparation of plasticized NaCMC/PEO/$LiClO_4$ electrolytes: A solution-casting method was utilized to fabricate a new plasticized Na CMC/PEO/$LiClO_4$ electrolyte. The polymer blend, consisting of Na CMC and PEO

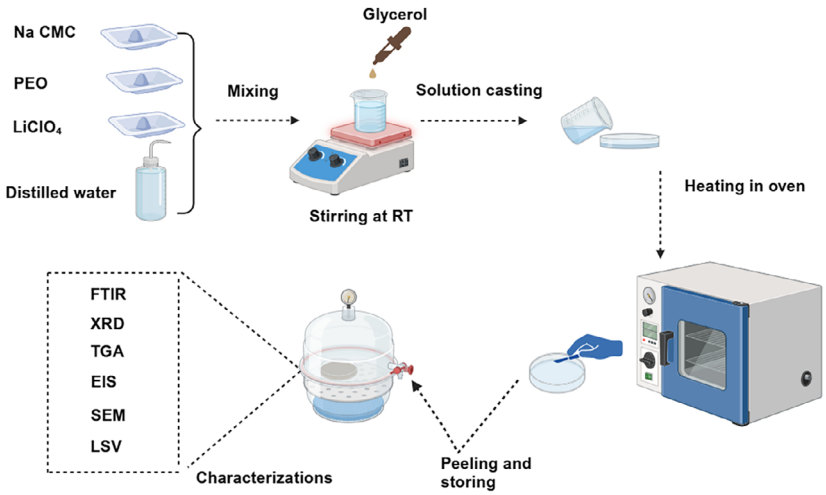

Scheme 1. Illustration of the experimental steps for the preparation of plasticized Na CMC/PEO/$LiClO_4$ electrolyte films.

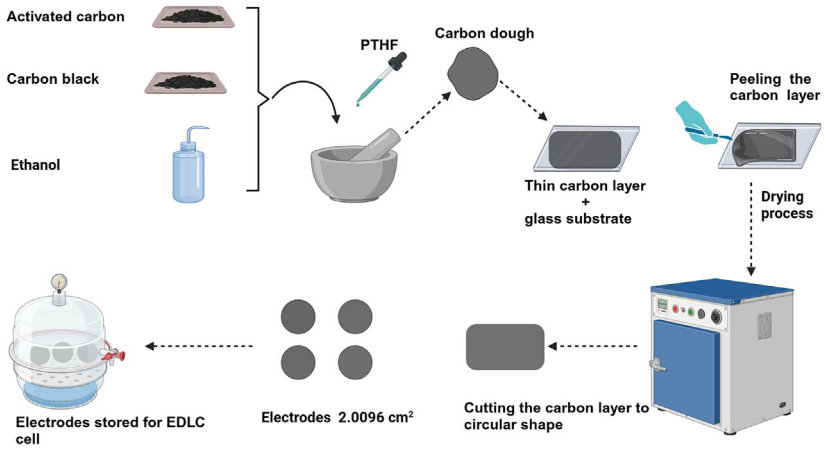

Scheme 2. Experimental steps of electrodes preparation.

with a total mass of 3 g and an 80:20 weight ratio, was utilized to prepare the samples. The amount of salt added was calculated using the Equation (17).

$$LiClO_4\ (\text{wt.}\%) = \frac{m_s}{m_s + m_p + m_g} \times 100\% \quad (17)$$

Here m_s refers to the mass of $LiClO_4$, m_p is the mass of (Na CMC/PEO), and m_g represents the mass of the glycerol with a fixed amount of 1 g.

The polymer blend and the specified salt compositions (see **Table 3**) were each dissolved in 150 mL of distilled water and stirred continuously for 24 h. Subsequently, 1 g of glycerol was introduced into the solution, followed by an additional 4 h of stirring. The homogeneous solution was meticulously cast into Petri dishes and subjected to drying in an oven at 70 °C. Once drying was complete, the freestanding electrolyte films were gently removed and placed in a desiccator for subsequent characterization, as depicted in **Scheme 1**.

Preparation of electrodes and EDLC assembling: A total mass of 0.5 g was allocated for preparing the electrode materials, comprising 80 wt.% activated carbon, 10 wt.% carbon black, and 10 wt.% polytetrafluoroethylene (PTFE) in *N*-methyl-2-pyrrolidone (NMP). Accordingly, 0.4 g of activated carbon and 0.05 g of carbon black were mixed thoroughly in a laboratory mortar using a pestle until a homogeneous blend was achieved. Ethanol was then introduced and manually stirred until the solvent fully evaporated, yielding a cohesive slurry. Subsequently, 0.05 g of a PTFE binder solution was added and kneaded with a spoon spatula until the mixture achieved a dough-like consistency. This mixture was spread evenly over a glass substrate to form a thin carbon film. Following the formation of the film, it was carefully separated from the glass substrate using a razor blade and left to dry overnight in an oven. The dried carbon film was then trimmed into circular electrodes measuring 16 mm in diameter and approximately 0.1 mm in thickness. These films were stored in a desiccator for later use.

For the fabrication of the EDLC cell, the R20 sample was incorporated into a 2023-type coin cell according to the configuration shown in Figure 1c. To ensure optimal interfacial contact between all cell components, a uniform pressure of 90 kg cm^{-2} was applied using a digitally controlled, pressure-regulated electric crimper. The process is illustrated in **Scheme 2**.

Acknowledgements

This work was supported by the Internal Grant Agency of TBU in Zlin (IGA/CPS/2025/002), the Ministry of Education Youth and Sports of the Czech Republic—DKRVO (RP/CPS/2024-28/002). R.A.K. and V.S. further acknowledge support from the European Just Transition Fund within the Operational Programme Just Transition under the aegis of the Ministry of the Environment of the Czech Republic, project CirkArena number CZ.10.03.01/00/22_003/0000045 and Operational Programme Johannes Amos Comenius OP JAC "Application potential development in the field of polymer materials in the context of circular economy compliance (POCEK)", grant number CZ.02.01.01/00/23_021/0009004.

Conflict of Interest

The authors declare no conflict of interest.

Keywords

biomaterials, electrolytes, supercapacitors, sustainability

Received: January 28, 2025
Revised: March 21, 2025
Published online: March 27, 2025

[1] A. G. Olabi, Q. Abbas, A. Al Makky, M. A. Abdelkareem, *Energy* **2022**, *248*, 123617.
[2] R. A. Khellouf, S. Durpekova, V. Cyriac, J. Cisar, C. Bubulinca, A. Lengalova, D. Skoda, V. Sedlarík, *Solid State Ion.* **2023**, *402*, 116379.
[3] V. Cyriac, Ismayil, I. M. Noor, K. Mishra, C. Chavan, R. F. Bhajantri, S. P. Masti, *Cellulose* **2022**, *29*, 3271.
[4] J. Zhang, X. Yao, R. K. Misra, Q. Cai, Y. Zhao, *J. Mater. Sci. Technol.* **2020**, *44*, 237.
[5] J. R. Andrade, E. Raphael, A. Pawlicka, *Electrochim. Acta* **2009**, *54*, 6479.
[6] L. Jenova, K. Venkatesh, S. Karthikeyan, S. Madeswaran, G. Aristatil, M. Prabu, D. Joice Sheeba, *J. Solid State Electrochem.* **2021**, *25*, 2371.
[7] R. A. Khellouf, C. Bubulinca, V. Cyriac, J. Cisar, S. Durpekova, V. Sedlarik, *J. Energy Storage* **2024**, *101*, 113769.

[8] Z. Zheng, W. Shi, X. Zhou, X. Zhang, W. Guo, X. Shi, Y. Xiong, Y. Zhu, *iScience* **2023**, *26*, 106437.
[9] N. A. A. Ghani, R. Othaman, A. Ahmad, F. H. Anuar, N. H. Hassan, *Arab. J. Chem.* **2019**, *12*, 370.
[10] Sustainable Energy for All, Sustainable Development Goal 7 (SDG7). **2024**.
[11] C. Change, E. Energy, Zero Pollution Action Plan. **2024**.
[12] D. K. Verma, R. Tiwari, D. Kumar, S. Yadav, K. Parwati, P. Adhikary, S. Krishnamoorthi, *Mater. Sci. Eng. B* **2023**, *297*, 116800.
[13] B. H. Lim, J. M. Kim, V. T. Nguyen, H. Kim, C. W. Park, J. K. Lee, C. H. Lee, J. Yoo, B. K. Min, S. K. Kim, *Mater. Today Energy* **2023**, *33*, 101263.
[14] Z. Jia, Y. Liu, H. Li, Y. Xiong, Y. Miao, Z. Liu, F. Ren, *J. Energy Chem.* **2024**, *92*, 548.
[15] L. Herbers, J. Minář, S. Stuckenberg, V. Küpers, D. Berghus, S. Nowak, M. Winter, P. Bieker, *Adv. Energy Sustain. Res.* **2023**, *4*, 00153.
[16] J. Wang, Y. Zhang, Z. Chen, S. Fan, Q. Zhang, Y. Zhang, T. Zhang, C. Zhang, Q. Chi, *Chem. Eng. J.* **2024**, *492*, D152222.
[17] M. Salari, J. C. Varela, H. Zhang, M. W. Grinstaff, *Mater. Adv.* **2021**, *2*, 6049.
[18] N. A. Shamsuri, Z. E. Rojudi, V. T. Vicxeant, I. M. Noor, M. F. Z. Kadir, M. F. Shukur, *Ionics (Kiel)* **2023**, *29*, 4243.
[19] S. B. Aziz, O. G. Abdullah, R. T. Abdulwahid, M. J. Ahmed, H. B. Tahir, S. R. Saeed, M. F. Z. Kadir, *Electrochim. Acta* **2023**, *467*, 143134.
[20] G. Gopinath, P. Shanmugaraj, M. Sasikumar, M. Shadap, B. A, S. Ayyasamy, *Appl. Surf. Sci. Adv.* **2023**, *18*, 100498.
[21] S. B. Aziz, R. T. Abdulwahid, P. A. Mohammed, S. O. Rashid, A. A. Abdalrahman, W. O. Karim, B. A. Al-Asbahi, A. A. A. Ahmed, M. F. Z. Kadir, *J. Energy Storage* **2024**, *76*, 109730.
[22] S. B. Aziz, E. M. A. Dannoun, A. R. Murad, K. H. Mahmoud, M. A. Brza, M. M. Nofal, K. A. Elsayed, S. N. Abdullah, J. M. Hadi, M. F. Z. Kadir, *Alex. Eng. J.* **2022**, *61*, 5919.
[23] R. T. Abdulwahid, S. B. Aziz, M. F. Z. Kadir, *J. Energy Storage* **2023**, *67*, 107636.
[24] J. Huang, S. Wang, J. Chen, C. Chen, E. Lizundia, *Adv. Mater.* **2025**, 2416733.
[25] A. K. Arof, S. Amirudin, S. Z. Yusof, I. M. Noor, *Phys. Chem. Chem. Phys.* **2014**, *16*, 1856.
[26] Y. Tan, M. Xi, Y. Zhang, Z. Qiao, *J. Power Sources* **2024**, *624*, 235554.
[27] L. H. Sim, S. N. Gan, C. H. Chan, R. Yahya, *Spectrochim. Acta A Mol. Biomol. Spectrosc.* **2010**, *76*, 287.
[28] S. K. Shetty, S. Hegde, V. Ravindrachary, G. Sanjeev, R. F. Bhajantri, S. P. Masti, *Ionics* **2021**, *27*, 2509.
[29] M. H. Hamsan, M. F. Zamani Kadir, M. F. Aziz, M. F. Shukur, *Int. J. Hydrogen Energy* **2022**, *47*, 38690.
[30] A. A. Rahim, N. A. Shamsuri, A. A. Adam, M. F. Aziz, M. H. Hamsan, H. Rusdi, S. O. J. Siong, I. M. Noor, M. F. Z. Kadir, M. F. Shukur, *J. Energy Storage* **2024**, *97*, 112964.
[31] D. A. Darmawan, E. Yulianti, Q. Sabrina, K. Ishida, A. W. Sakti, H. Nakai, E. Pramono, S. T. C. L. Ndruru, *Polym. Compos.* **2024**, *45*, 2032.
[32] Y. Li, W. Yuan, F. Lu, Y. Shen, D. Li, F. Cong, P. Zhu, Y. Li, P. Liu, Y. Huang, J. Li, Z. Hu, *Small* **2024**, *20*, 202405187.
[33] M. H. Hamsan, M. F. Shukur, M. F. Z. Kadir, *Ionics (Kiel)* **2017**, *23*, 1137.
[34] R. Baskaran, S. Selvasekarapandian, N. Kuwata, J. Kawamura, T. Hattori, *J. Phys. Chem. Solid* **2007**, *68*, 407.
[35] M. Ejder-Korucu, A. Gürses, S. Karaca, *Appl. Surf. Sci.* **2016**, DOI: https://doi.org/10.1016/j.apsusc.2016.03.159.
[36] M. A. Rahman, M. A. Khan, S. M. Tareq, *J. Appl. Polym. Sci.* **2010**, *117*, 2075.
[37] A. L. Waly, A. M. Abdelghany, A. E. Tarabiah, *J. Mater. Res. Technol.* **2021**, *14*, 2962.
[38] S. Yang, Z. Liu, Y. Jiao, Y. Liu, W. Luo, *J. Mater. Sci.* **2013**, *48*, 6811.
[39] C. M. D. Winn, P. Patel, E. Krissinel, Developments in Data Harvesting Within. n.d.
[40] S. Park, J. O. Baker, M. E. Himmel, P. A. Parilla, D. K. Johnson, *Biotechnol. Biofuels* **2010**, *3*, 10.
[41] V. Cyriac, K. Ismayil, K. Mishra, A. Rao, S. P. Masti, I. M. Noor, *Electrochim. Acta* **2024**, *507*, 145139.
[42] S. B. Aziz, O. G. Abdullah, D. M. Aziz, M. B. Ahmed, R. T. Abdulwahid, *ACS Appl. Electron. Mater.* **2024**, *6*, 7763.
[43] J. C. Barbosa, R. S. Pinto, D. M. Correia, C. R. Tubio, R. Gonçalves, C. M. Costa, S. Lanceros-Mendez, *J. Power Sources* **2023**, *585*, 233630.
[44] V. Cyriac, I. S. B. M. Ismayil, Z. E. Noor, Y. N. Rojudi, C. Sudhakar, R. F. Chavan, M. S. Bhajantri, Murari, *Int. J. Energy Res.* **2022**, *46*, 22845.
[45] V. Cyriac, Y. N. Ismayil, Y. N. Sudhakar, K. Mishra, Z. E. Rojudi, M. S. Murari, I. M. Noor, *Mater. Res. Bull.* **2024**, *169*, 112498.
[46] V. Cyriac, K. Ismayil, K. Mishra, Y. N. Sudhakar, Z. E. Rojudi, S. P. Masti, I. M. Noor, *Solid State Ion.* **2024**, *411*, 116578.
[47] A. Rao, S. Bhat, S. De, V. Cyriac, *J. Energy Storage* **2024**, *102*, 113965.
[48] S. A. M. Noor, A. Ahmad, I. A. Talib, M. Y. A. Rahman, *Ionics (Kiel)* **2010**, *16*, 161.
[49] M. Muthuvinayagam, C. Gopinathan, *Polymer (Guildf)* **2015**, *68*, 122.
[50] Y. L. Yap, A. H. You, L. L. Teo, H. Hanapei, *Int. J. Electrochem. Sci.* **2013**, *8*, 2154.
[51] M. F. Z. Kadir, S. R. Majid, A. K. Arof, *Electrochim. Acta* **2010**, *55*, 1475.
[52] M. Akram, I. Taha, M. M. Ghobashy, *Cellulose* **2016**, *23*, 1713.
[53] M. S. A. Rani, S. Rudhziah, A. Ahmad, N. S. Mohamed, *Polymers (Basel)* **2014**, *6*, 2371.
[54] A. A. Ibrahim, A. M. Adel, Z. H. A. El-Wahab, M. T. Al-Shemy, *Carbohydr. Polym.* **2011**, *83*, 94.
[55] B. Asbani, C. Douard, T. Brousse, J. Le Bideau, *Energy Storage Mater.* **2019**, *21*, 439.
[56] A. Likitchatchawankun, G. Whang, J. Lau, O. Munteshari, B. Dunn, L. Pilon, *Electrochim. Acta* **2020**, *338*, 135802.
[57] E. Calabrò, S. Magazù, *Phys. Lett. A* **2018**, *382*, 1389.
[58] S. B. Aziz, P. O. Hama, P. A. Mohammed, M. B. Ahmed, R. M. Abdullah, N. M. Sadiq, M. F. Z. Kadir, H. J. Woo, *J. Energy Storage* **2024**, *103*, 114264.
[59] L. Li, N. Lu, D. Jiang, Z. Chen, W. Zhang, W. Zheng, X. Zhu, G. Wang, *J. Colloid Interface Sci.* **2021**, *586*, 110.
[60] K. Sun, X. Shi, X. Xie, W. Hou, X. Wang, H. Peng, G. Ma, *Int. J. Biol. Macromol.* **2025**, *286*, 138376.